VESICLE SHAPES AND SHAPE TRANSFORMATIONS:
A SYSTEMATIC STUDY

Karin Berndl[1], Josef Käs[2], Reinhard Lipowsky[1],
Erich Sackmann[2] and Udo Seifert[1]

1. Sektion Physik der Universität München
   Theresienstr. 37, 8000 München 2 (FRG)
2. Technische Universität München, Physik
   Department, Biophysics Group (E22)
   8046 Garching (FRG)

1. INTRODUCTION

The lipid bilayer vesicle is the simplest possible model of biological membranes. Nevertheless, it exhibits already a number of typical properties of cell membranes. The most fascinating examples are the shape transitions and shape instabilities. It has been recognized long ago that shape transitions may be induced by changing the osmotic conditions or the temperature[1]. Apart from spherical and ellipsoidal shapes more exotic shapes such as e.g. discocytes, stomatocytes[1], echinocytes[2] or a necklace of small vesicles[3] has recently been observed. Up to now, our understanding of these shape transformations has been rather limited. Indeed, all previous experiments have been performed with relatively complex systems containing, e.g. charged and unsaturated lipids, mixtures of different lipids or additional solutes such as sugar in the aqueous phase. It was generally believed that these different ingredients play an essential role in determining the vesicle shape. Therefore, no attempt has been reported so far to relate these experimentally observed shapes in a systematic way to theoretical calculations.

In our contribution we report a systematic experimental and theoretical study on these shape transformations. In order to avoid the above mentioned complications we have investigated vesicles which consist of electrically neutral lipids (that is phosphatidylcholine) in Millipore water. We find, that even for such a simple system a change in temperature can lead to three different types of shape transformations. Theoretically, we discuss shape transformations within two well established curvature models, (i) the bilayer coupling model of Svetina and Zeks[4] and (ii) the spontaneous curvature model of Helfrich[5,6]. A comparison leads to the conclusion that the observed shape transformations can well be explained within the bilayer coupling model provided a small asymmetry in the thermal expansivities of both monolayers is assumed. In some cases, such an asymmetry is not required.

2. EXPERIMENTAL SETUP

Our experiments were performed with vesicles of dipalmitoylphosphatidylcholine (DMPC) of diameters larger than 20 μm. These were prepared in a separate test-tube. The lipid with a purity >99% was dissolved in a solvent of 2:1 chloroform/methanol to produce a 1 mM solution. Then, 60 μl of this solution were distributed as a thin film on the inner surface of the test-tube. The solvent was evaporated by placing the test-tube in a vacuum chamber for a minimum of one day. Then the vesicles were swollen by filling the test-tube with 5 ml distiled water prepared with a Milli-Q-System and heating the solution up to 40°C.

After swelling for a minimum of 12 hours, the vesicles were transferred into a special chamber which allows, for the first time, the observation of free vesicles without being driven off by thermal convection. A schematic view of this measuring chamber is shown in Fig.1. The hollow outer copper frame is used to cool and heat the chamber with a water thermostat. The inner frame is made of teflon and a temperature sensor (Pt 100) is integrated in this frame. The top and bottom of the chamber are closed with cover slides. These were fixed with vacuum grease. An inner compartment is placed onto the bottom cover slide. It is formed by a thin teflon spacer (open at one side) covered by a small cover slide. The inner
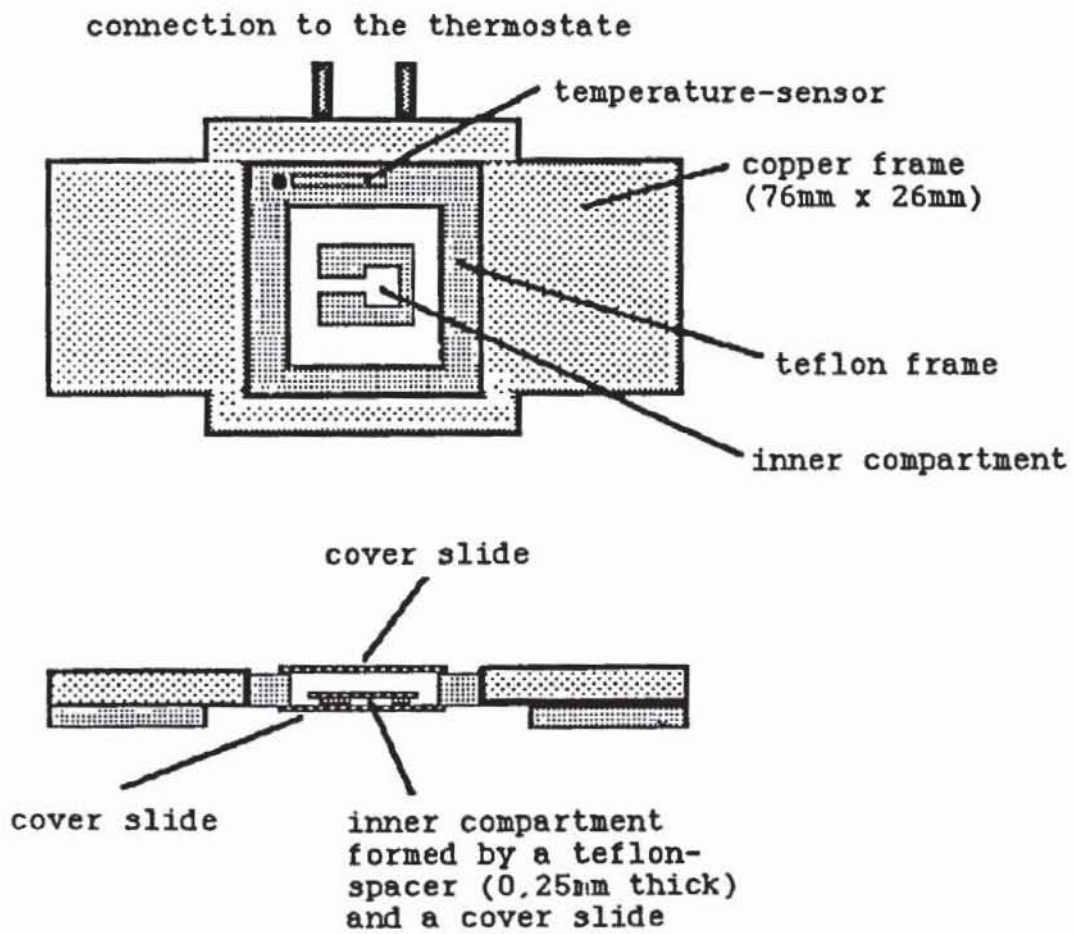
connection to the thermostate

temperature-sensor

copper frame
(76mm x 26mm)

teflon frame

inner compartment

cover slide

cover slide

inner compartment
formed by a teflon-
spacer (0.25mm thick)
and a cover slide

Fig.1. Measuring chamber with an inner (dead water) confine-
ment to prevent swimming away of freely suspended vesi-
cles by thermal convection.

compartment is essentially free of thermal convection and for this reason it is used for the observation of the vesicles. The outer compartment is required for a good thermal coupling to the thermostated frame. The vesicles were observed in phase contrast with an inverted Zeiss Axiovert 10 microscope. For the present work, a bright field air objective of magnification 40x (Zeiss) was used. During the slow increase of the temperature ≈ 0.2 K/min, the volume and the area of the observed vesicle were measured with a digital image processing system (Maxvideo, Datacube Boston, USA). The details of measuring the volume and the area will be described elsewhere[7].

3. THREE DIFFERENT TYPES OF SHAPE TRANSFORMATIONS

In our experiments we normally started with spherical or ellipsoidal vesicles of a size between 20 μm and 50 μm, which are most suitable to determine the initial values of the volume and the surface area. We found the following different types of shape transformations caused by increasing the temperature: Firstly, the budding transition exhibiting the following evolution: The sphere changes into a prolate ellipsoid and then into a pear-shaped state, which finally forms a vesicle with one bleb on the outside (see Fig.2). The second type is a reentrant shape transformation. One first obtains a prolate ellipsoid, which changes into a dumbbell shape, then into a pear-shaped state and again into a dumbbell-shaped state (see Fig.3). The third type is the discozyte-stomatozyte transition. The first step is the change from a sphere to a oblate ellipsoid. The ellipsoid changes into a discozyte and finally into a stomatozyte (see Fig.4). The last transition is completely analogous to the discocyte-stomatocyte transition of red blood cells and provides convincing evidence for our introductory remark that most simple bilayer vesicle may mimic typical behaviors of the complex biological membranes. This suggests that shape changes of biological membranes are governed by simple principles.

In Fig. 2-4, we compare the three types of experimentally observed shape transformations with shape changes, calculated with the theoretical model described below. The three

theoretical sequences differ mainly in the value of a
dimensionless parameter, γ, which measures the asymmetry in the
thermal expansivities of the two monolayers. If the thermal
expansivity of the outer monolayer is larger than the inner
one and exhibits a relative difference $\gamma \geq 10^{-2}$, a small vesicle
buds off the large vesicle. For $0 \leq \gamma \leq 10^{-3}$ the reentrant
transitions from a dumbbell to a pear-shaped state occurs,
while a larger expansivity of the inner monolayer leads to the
discozyte-stomatozyte transitions and finally to the formation
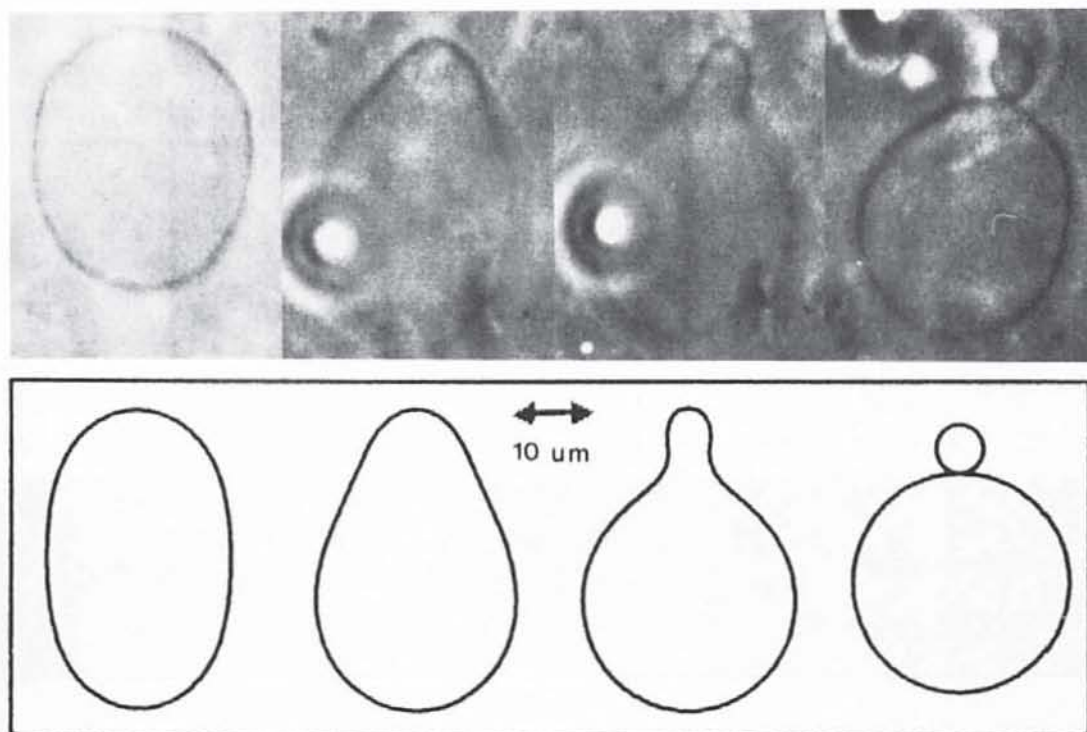of a small vesicle budding towards the inside.

Fig.2. Demonstration of a budding transition: The shapes were
measured at $T = 31.4$, 35.5, 35.6 and 35.8^0C. The disc-
like object is due to an air bubble which migrates in
the outer compartment of the measuring chamber. The
calculated shapes correspond to a trajectory of Eqs.(4)
with initial values of the reduced volume $v_0 = 0.9446$
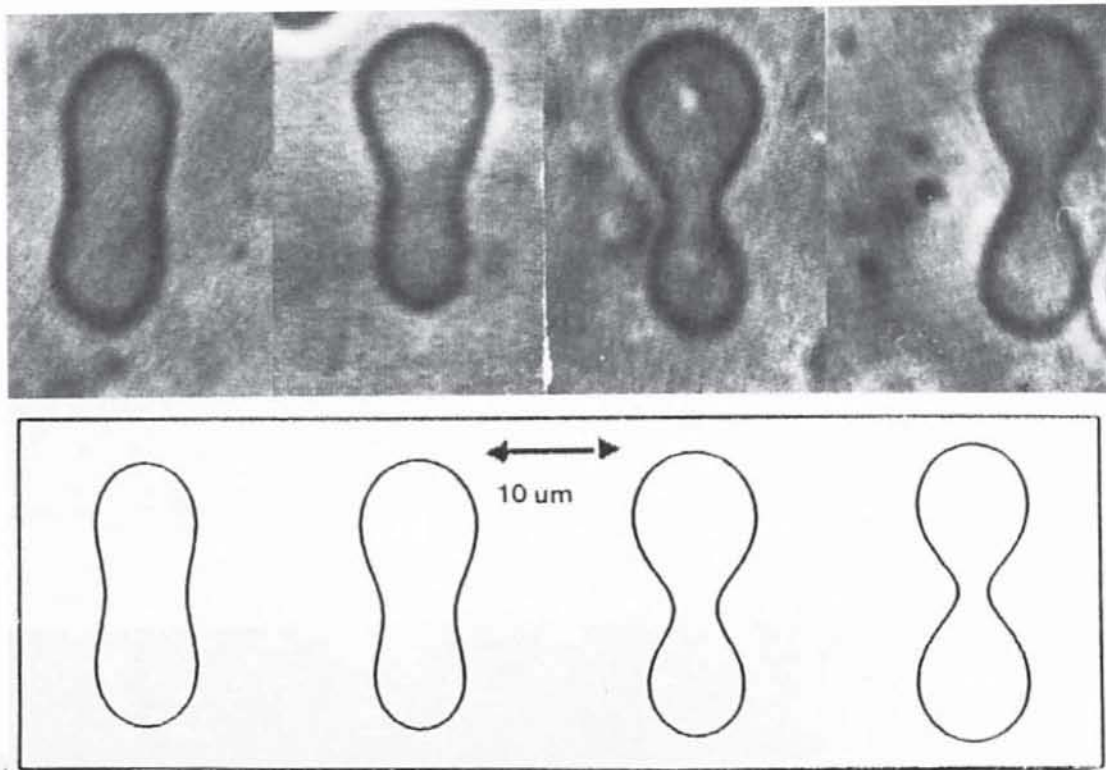and reduced area difference $\Delta a_0 = 1.0305$, $\gamma = 0.057$ and
$b = 1500$.

Fig.3. Symmetric-asymmetric reentrant transition: The shapes were measured at T = 30.7, 32.6, 40.0 and 44.3^{0}C. The calculated shapes correspond to a trajectory of Eqs.(4) with v_0 = 0.78, Δa_0 = 1.1475, γ = 0.00166 and b = 640.
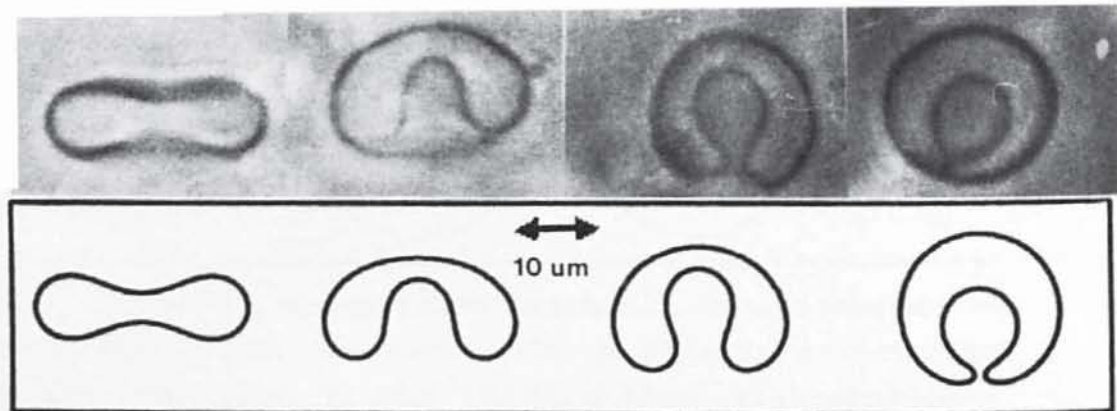

Fig.4. Discocyte-stomatocyte transition: The shapes were measured at T = 43.8, 43.9, 44.0 and 44.1^{0}C. The calculated shapes correspond to a trajectory of Eqs.(4) with v_0 = 0.65, Δa_0 = 1.0355, γ = -0.29 and b = 1000.

4. THEORETICAL MODELS AND THEIR AGREEMENT WITH THE EXPERIMENT

For a comparison of the experimental results with theoretical ideas, we calculated shapes and shape transitions within two variants of curvature models: (i) the bilayer coupling model of Svetina and Zeks[4], (ii) the spontaneous curvature model of Helfrich[5,6]. We first discuss the bilayer coupling model. Within this model, the two monolayers are taken to be infinite thin shells with a constant separation D, where D is about the half bilayer thickness. The shape of the vesicle is determined by the minimum of the bending energy, G_b,

$$G_b = (\kappa/2) \oint (C_1 + C_2)^2 \, dA^{in} \tag{1}$$

which is expressed as an integral over the inner monolayer only since both monolayers are coupled. It is convenient to express all equations in terms of the surface areas A^{in} and A^{ex} rather than in terms of the neutral surface. Here, κ denotes the effective bending rigidity of the bilayer with $\kappa \approx 1.15 \times 10^{-19}$ J for DMPC[8]. The variables $C_1 = 1/R_1$ and $C_2 = 1/R_2$ are the two principal curvatures expressed by the two radii of curvature R_1 and R_2. The area difference $\Delta A \equiv A^{ex} - A^{in}$ of both monolayers is related to the total mean curvature of the inner monolayer via $\Delta A \approx D \int (C_1 + C_2) \, dA^{in}$ for small values of d. The minimization of G_b is now performed for fixed area A^{in}, fixed enclosed volume V, and fixed area difference ΔA. Thus, we assume that the exchange of lipid molecules between both monolayers can be ignored on experimentally relevant periods. This minimization leads to the shape equation

$$\delta \left[G_b + \Sigma A + PV - \frac{\kappa}{D} C_0 \Delta A \right] = 0 \tag{2}$$

where δ denotes the variation with respect to the vesicle shape and Σ', P and C_0 denote Lagrange multipliers which can be identified with the lateral tension, the pressure difference and the spontaneous curvature, respectively.

For the model just described, we have determined the "phase diagram"[9], i.e., we have determined the axi-symmetric
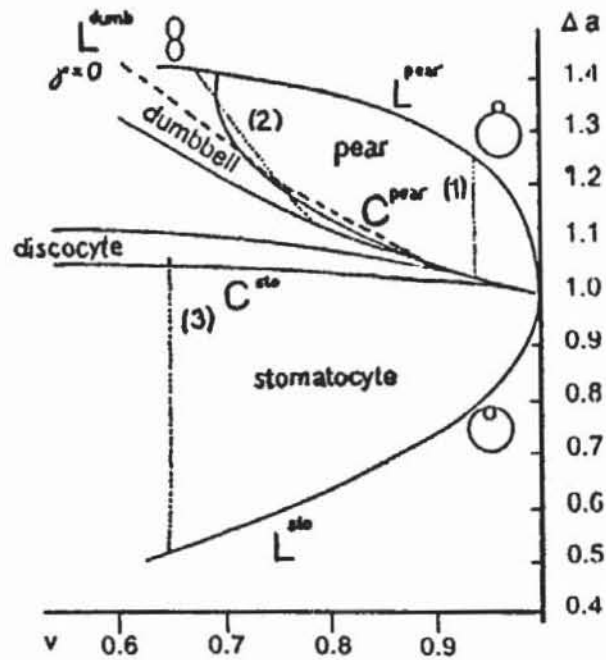
Fig.5. Phase diagram and temperature trajectories for the bi-layer coupling model. This phase diagram shows the state of lowest energy for given Δa and υ. C^{pear} and C^{sto} denote lines of continuous transitions at which the up/down symmetry of the vesicle shape is broken. L^{pear}, L^{sto} and L^{dumb} denote limit shapes. Note that the dumbbell region contains for large υ-values prolate ellipsoids and that the discocyte region contains for large υ-values oblate ellipsoids. The pointed lines (1), (2) and (3) represent the temperature trajectories for Fig.2, Fig.3 and Fig.4. The dashed line represents the temperature trajectory for the asymmetry parameter $\gamma = 0$ with $\upsilon_0 = 0.9$ and $\Delta a_0 = 1.05$.

shapes of lowest bending energy for experimentally accessible
values of the reduced volume υ with

$$\upsilon \equiv V / \left[(4\pi/3) \; (A^{in}/4\pi)^{3/2} \right] \qquad (3)$$

which is a measure for the excess area and the induced area
difference Δa with

$$\Delta a \equiv \Delta A / \left[8\pi \; D \; (A^{in}/4\pi)^{1/2} \right] \qquad (4)$$

For a sphere, one has $\upsilon = \Delta a = 1$. This phase diagram is dis-
played in Fig.5. Some part of it has been previously described
by Svetina and Zeks[4]. As two important novel features, we find
(i) an instability of the dumbbell shapes with respect to the
up/down symmetry which leads to the pear-shaped states, and
(ii) new limiting shapes which look like two prolate ellip-
soids sitting on top of each other.

In order to compare theoretical and experimental shapes,
we determine the path $\Delta a = \Delta a(\upsilon)$ which corresponds to a change
in temperature T. We now assume that the interior and exterior
monolayer have different temperature independent relative ex-
pansivities, α^{in} and α^{ex}, as given by

$$\alpha^{in} \equiv \frac{1}{A^{in}} \frac{dA^{in}}{dT} \text{ and } \alpha^{ex} \equiv \frac{1}{A^{ex}} \frac{dA^{ex}}{dT} , \text{ with } \alpha^{ex} = (1 + \gamma) \alpha^{in} . \qquad (5)$$

For simplicity, we neglect the small thermal expansivity of
the enclosed water. We assume that the thermal expansivity of
D is given by $(-1/2)\alpha^{in}$ [10]. Differentiating Eqs.(3) with re-
spect to the temperature T and inserting Eqs.(5) leads after
integration to the temperature dependence of the reduced vol-
ume as given by

$$\upsilon(T) = \upsilon_0 \exp\{(-3/2) \; \alpha^{in} \; (T - T_0)\} \qquad (6)$$

where $\upsilon_0 = \upsilon(T_0)$ defines the initial value. A similar equation
can be derived for $\Delta a(T)$. If $(T - T_0)$ is eliminated in both
equations one finds the temperature trajectory

$$\Delta a(\upsilon) = \left(\frac{\upsilon_0}{\upsilon}\right)^{2/3} \left[\Delta a_0 + b\left(\left(\frac{\upsilon_0}{\upsilon}\right)^{2\gamma/3} - 1 \right) \right], \qquad (7)$$

103

where $v_0 \equiv v(T_0)$ and $\Delta a_0 \equiv \Delta a(T_0)$ parametrized the initial shape at temperature $T = T_0$ and

$$b \equiv A^{ex}(T_0)/\{8\pi\, D(T_0)\, [A^{in}(T_0)/4\pi]^{1/2}\} \qquad (8)$$

For $\gamma = 0$, i.e., if the asymmetry were not present, the second term in Eqs.(7) vanishes and a temperature trajectory in the phase diagram would be given by $\Delta a(v) = (v_0/v)^{2/3}\Delta a_0$. This path is shown as a dashed line in Fig.4: Starting, e.g. with a symmetric prolate ellipsoid, it immediately crosses the phase boundary C^{pear} and enters the pear-shaped region; it then crosses again the line of continuous transitions C^{pear} and finally meets the new type of limiting shapes at L^{dumb}. Note that such a path never enters the stomatocyte region. Any $|\gamma|$ in the order of 10^{-3}, however, has already a significant influence since the parameter b as given by Eqs.(8) can be estimated to be of orders 10^3 for the typical values $A^{in}(T_0) \approx A^{ex}(T_0) \approx 1000\ \mu m^2$ and $D \approx 5$ nm.

The asymmetry γ and the initial area difference Δa_0 cannot be measured or controlled directly in our experiment. A crude estimate, however, can be obtained by comparing the experimental with theoretical shapes. The calculated shapes shown in Fig. 2-4 lie on a trajectory described by Eqs.(4) within the experimentally observed temperature intervals. For Fig.3 and Fig.4, the parameters b, v_0, Δa_0 and γ were obtained as follows: The measured area A and volume V of the first shape at temperature T_0 determines v_0 and b, where we used $A^{in} \approx A^{ex} \approx A$ and $D \approx 5$ nm. The area difference Δa_0 is chosen to fit the experimental shape. The measured temperature interval $T_f - T_0$ between the final and the initial shape determines $v(T_f)$ via Eqs.(6) with $\alpha^{in} \approx 6 \times 10^{-3}$ [12]. Once again, $\Delta a(T_f)$ is fitted to the experimental shape, which finally determines the value of the asymmetry parameter γ. For Fig.2, we first determined $v(T_f)$ from the last shape and then $v(T_0)$ from the measured temperature difference to the second shape.

Although the experimental and theoretical results agree very well, it is worthwhile to envisage also an explanation within the spontaneous curvature model. Within this model the shape of the vesicle with given area A and enclosed volume V is determined by the minimum of the bending energy F_b, with

$$F_b = (\kappa/2) \oint (c_1 + c_2 - c_0)^2\, dA, \qquad (9)$$

The microscope details of the two monolayers are described by the spontaneous curvature C_0. The minimization leads to the same shape equation as Eqs.(2) and consequently to the same extremal shapes. A shape which corresponds to a local minimum of G_b, may, however, correspond to a local maximum of F_b. Therefore the phase diagram in both models are quite different. The phase diagram for the spontaneous curvature model depends on υ given by Eqs.(3) and the reduced spontaneous curvature

$$c_0 \equiv C_0 \ (A/4\pi)^{1/2} \tag{10}$$

We display, the phase diagram in Fig.6. Its derivation will be presented elsewhere[9]. Its main characteristics are:
1) For $C_0 \geq 2.08$, a discontinuous transition D^{pear} separates prolate/dumbbell from pear-shaped states.
2) With decreasing volume, the pear-shaped vesicles become symmetric again for $C_0 < 2\sqrt{2}$ at C^{pear}.
3) For $C_0 > 2\sqrt{2}$, however, the pear-shaped vesicles reach a limit-shape L^{pear} with decreasing volume. This limit shape consists of two spheres which are connected by an narrow neck, which contains no energy since the two curvatures have compensating signs. Such an "ideal" neck is only possible if the radii R_1 and R_2 of the two spheres fulfil the relation

$$R_1^{-1} + R_2^{-1} = C_0 \tag{11}$$

This equation, together with the conservation of area 4π $[R_1^2 + R_2^2] = A$, determines which spontaneous curvature C_0 is necessary in order to obtain budding of a smaller vesicle with radius R_1. For small R_1, we have $C_0 \approx R_1^{-1}$.
4) A discontinuous transition D^{sto} leads from oblate/discocyte shapes to the stomatocytes. For $C_0 < 0$, these shapes reach a limit shape L^{sto} given by an inverted sphere of radius $R_1 < 0$ embedded in a large sphere of radius $R_2 > 0$. Once again Eqs.(11) holds for the limit shape.

In order to compare this phase diagram and the predicted transitions with the experimental trajectory, we need the temperature dependence of C_0, which is not clear a priori. We therefore assume that C_0 remains temperature independent. For
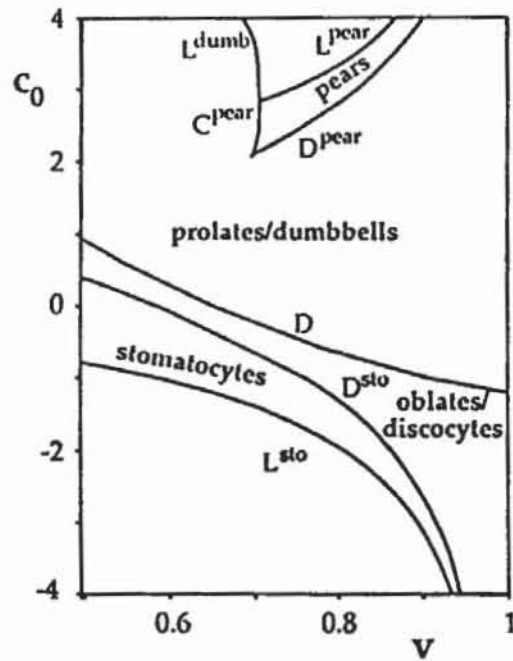
Fig.6. Phase diagram for the spontaneous curvature model. This phase diagram shows the state of lowest energy for given c_0 and v. C^{pear} denotes a line of continuous transition at which the up/down symmetry of the vesicle shape is broken. D^{pear}, D and D^{sto} denote lines of discontinuous transitions. L^{pear}, L^{sto} and L^{dumb} denote limit shapes.

the volume, Eqs.(6) remains valid. Let us now discuss which theoretical trajectories could fit the experimentally observed ones:

(1) For a reentrant trajectory as in Fig.3, the spontaneous curvature model predicts a discontinuous transition from the symmetric to the pear-shaped state. Of course, the distinction between a continuous and a discontinuous transition for a single vesicle is experimentally difficult. For a discontinuous transition, one expects a strong variation of the shape within a short time caused by an infinitely small change of the area and the occurrence of hysteresis. The observed reentrant trajectory, however, occurred over a relative large temperature interval of 14 K, which corresponds to a time interval of 70 min. A further objection against the spontaneous curvature model for this trajectory is that the neck at the C^{pear}-line is significantly narrower for the calculated shapes than for to the experimental ones.

(2) In order to obtain a budding trajectory leading to a bleb of the observed small size a spontaneous curvature $C_0 \approx 5-6$ has to be postulated. which is rather improbable for our pure system. Moreover, all budding trajectories in the spontaneous curvature model should be precursed by the first order transition from the symmetric to the pear-shaped states.

(3) Finally, the discocyte-stomatocyte transition in this model is first order and would require a negative spontaneous curvature to occur for the observed υ-value.

Summarizing, the detailed analysis of the phase diagram for both models allows to test critically whether these models apply to the observed shape transformations. We find that the bilayer coupling model augmented with an asymmetry in the monolayer expansivity fits well while the spontaneous curvature models makes qualitatively different predictions. Especially, we consider the transition from a prolate ellipsoid to a pear-shaped state in Fig.2 and the discocyte-stomatocyte transition in Fig.4 as continuous. This is in accordance with the bilayer coupling model, but in disagreement with the spontaneous curvature model.

5. POSSIBLE REASONS FOR THE ASYMMETRY IN THE THERMAL EXPANSIVITIES

What could be the origin of the different thermal expansivities of the two monolayers? One possibility could be impurities such as lyso-lipids asymmetrically distributed between the both monolayers. A second more likely explanation is that the asymmetry is induced during the swelling process or the cooling of the vesicles from 40°C to room temperature during the transfer to the measuring chamber. Experimentally we found that after a long swelling time (about 24 hours) there is a preference for γ-values close to zero indicating a relaxation process. Further more the route of shape change depends on the lipid structure. For palmitoyloleylphosphatidylcholine (POPC), for instance, the values of $|\gamma|$ are remarkable higher. If an nearly spherical vesicle is cooled, so that a lateral stress is exerted within the bilayer, a high γ value arises. Thus heating, the vesicle again leads to a budding transition owing to a high value of γ. This example is shown in Fig. 2.

6. SUMMARY

The shape changes of giant bilayer vesicles consisting of phosphatidylcholine (DMPC) in pure water were studied. They were induced by temperature variations resulting in a change of the excess surface area since the volume remains essentially constant. Three different types of shape transformations were observed: firstly, a budding of small vesicles towards the outside of large vesicles which leads to a stepwise formation of a chain of vesicles at further increasing the temperature; secondly, a reentrant transition form a dumbbell to a pear-shaped state and thirdly, an oblate ellipsoid-discocyte-stomatocyte transition.

The shape transitions and the degree of continuity (order) can be best explained in terms of the bilayer coupling approach of Zeks and Svetina[4]; by assuming that the thermal expansivities of the two monolayers are different. The type of shape change depends on the asymmetry in the thermal expansivities of both monolayers. We provide evidence that the asymmetry in the case of symmetric bilayer vesicles (equal composition of outer and inner aqueous phases) is introduced

during preparation and that the route of transition depends also on the pretreatment of the vesicles. Our observations can be less well explained by the spontaneous curvature approach of Helfrich[5,6].

REFERENCES

1. E. Sackmann, H. P. Duwe and H. Engelhardt, Membrane bending elasticity and its role for shape fluctuations and shape transformations of cells and vesicles, *Faraday Discuss.Chem. Soc.* 81:468 (1986).

2. H. Gaub, R. Rüschl, H. Ringsdorf and E. Sackmann, Phase transitions, lateral phase seperation and microstructure of model membranes composed of a polymerizable two-chain lipid and dimyristoylcholine, *Chem.Phys.Lipids* 37:19 (1985)

3. E. Evans and W. Rawicz, Entropy-driven tension and bending elasticity in condensed-fluid membranes, *Phys.Rev.Lett.* 64:2094 (1990).

4. S. Svetina and B. Zeks, Membrane bending energy and shape determination of phospholipid vesicles and red blood cells, *Eur.Biophys.J.* 17:101 (1989).

5. W. Helfrich, Elastic properties of lipid bilayers, *Z.Naturforsch.* 28c:693 (1973).

6. H. J. Deuling and W. Helfrich, The curvature elasticity of fluid membranes: A catalogue of vesicle shapes, *J.Physique* 37:1335 (1976).

7. J. Käs and E. Sackmann, to be published.

8. H. P. Duwe, J. Käs and E. Sackmann, Bending elasticity moduli of lipid bilayers: modulation by solutes, *J.Physique* 51:945 (1990).

9. U.Seifert, K.Berndl and R.Lipowsky, to be published.

10. G. Cevc and D. Marsh, Bilayer thermomechanics and thermal expansion, in: *Phospholipid bilayers*, G. Cevc and D. Marsh, ed., John Wiley & Sons, New York, Chichester, Brisbane, Toronto, Singapore (1987).

11. E. Evans and D. Needham, Surface-Density Transitions, Surface Elasticity and Rigidity, and Rupture Strength of Lipid Bilayer Membranes, in: *Physics of Amphiphilic Layers, Springer Proceedings in Physics 21*, J. Meunier, ed., Springer, New York, Heidelberg, Berlin (1987).